AUT Journal of Electrical Engineering

AUT J. Elec. Eng., 58(Special Issue 1) (2026) 27-38
DOI: 10.22060/eej.2025.24292.5674

High-Precision Direction of Arrival Estimation for Closely Spaced Targets Using Binary-Phase Reconfigurable Intelligent Surfaces and Minimum Redundancy Linear Arrays

Meysam Raees Danaee*, Ahmad Ataei

Department of Electrical Engineering, Faculty of Electrical Engineering, Imam Hossein University, Tehran, Iran.

ABSTRACT: A novel method for enhancing the accuracy of direction of arrival estimation for two closely spaced targets by optimizing the geometric array configuration of a Binary-Phase Reconfigurable Intelligent Surface based on Minimum Redundancy Linear Arrays is proposed. In Binary-Phase Reconfigurable Intelligent Surfaces, the phases of the reflected signals at the Reconfigurable Intelligent Surfaces elements remain unchanged or undergo a 180-degree phase shift, making it significantly more cost-effective in terms of hardware compared to traditional direction of arrival estimation systems. This cost reduction, however, leads to an increase in the correlation of dictionary atoms. To compensate for this drawback, we regularize the optimization problem using atomic norm. Subsequently, the problem is transformed into its dual form to facilitate solving with existing solvers. Simulation results demonstrate that the proposed method can estimate the direction of arrival with higher accuracy for closely spaced targets in the angular domain, compared to existing Reconfigurable Intelligent Surfaces-based array methods, while maintaining the same hardware complexity.

Review History:
Received: Jun. 15, 2025
Revised: Oct. 19, 2025
Accepted: Nov. 07, 2025
Available Online: May, 05, 2026

Keywords:
DOA Estimation
Binary-Phase Reconfigurable Intelligent Surface (Binary-Phase RIS)
Minimum Redundancy Linear Arrays (MRLAs)
Atomic Norm Regularization

1- Introduction

Recently, reconfigurable intelligent surfaces (RIS) [1] have been widely studied in the fields of wireless communication, signal processing, and radar [2]. Given that RIS can intelligently and programmatically reflect signals and alter the amplitude or phase of the received signal, it can be used to expand signal coverage and enhance signal quality. This is particularly useful in scenarios where there is no direct line-of-sight between the transmitter and receiver, or where multipath fading is severe. The elements of RIS are essentially several varactor diodes or positive intrinsic negative (PIN) diodes, and their values are updated by the control channel as the wireless environment changes. However, in [3], the authors propose MARISA, a self-configuring metasurface solution that aims to operate without requiring constant adjustments to the RIS measurement matrix by a control channel as the wireless channel conditions change.

On the other hand, direction of arrival (DOA) estimation plays a crucial role in wireless communications. Given that RIS has low maintenance costs and, unlike traditional array structures, it can estimate the angle of arrival with only a limited number of discrete phase shifts, it presents a viable option for positioning and signal angle estimation. Another advantage of using RIS for estimating the angle of the received signal is that in environments where there is no direct line-of-sight (LOS) between the transmitter and receiver, RIS can be strategically placed in a location that has LOS with both the targets and the receiver. This allows for the accurate estimation of the angle of arrival of the signal at a receiver equipped with only a single antenna.

Unlike most papers, which approach the calculation of the elements of the RIS measurement matrix by solving an optimization problem to maximize the quality of service (QoS) or the received SNR in specific reception and transmission directions, [4] represents the first effort in this domain to tackle the selection of element values from the perspective of reducing correlation between the columns of the RIS measurement matrix, rather than enhancing SNR. To this end, a genetic algorithm is employed to design a matrix such that the correlation between any two rows is less than $\frac{1}{(2K+1)}$, where K represents the number of targets or the sparsity degree of the vector that needs to be recovered. Its results for DOA estimation have been promising. In [5], the authors have addressed DOA estimation by introducing a new atomic norm without knowing the element values of the

*Corresponding author's email: mraeesdanaee@ihu.ac.ir

measurement matrix and without the need for its optimization. They have extended their idea for the array structure in [6], assuming that the positions of the RIS elements have uncertainties following a Gaussian distribution.

To mitigate the need for complex data recovery techniques, such as sparse minimization problems or exhaustive grid search, in the estimation of DOA for a source with RIS in non-line-of-sight (NLOS) propagation, [7] proposes a polarized architecture. However, this solution necessitates the incorporation of more costly and intricate hardware in both the Base Transceiver Station (BTS) and the Reconfigurable Intelligent Surface (RIS), as it requires the installation of Electromagnetic Vector Sensor (EMVS) arrays arbitrarily placed at both locations. The concept of RIS-Aided DOA is explored in [8] and [9]. Considering an array structure instead of a single antenna configuration for the receiver, [10] also uses learning-based methodology for DOA estimation with RIS.

The accuracy of DOA estimation is influenced by the sensor array's configuration. Optimizing the geometry of the antenna array (e.g., arrays that are non-uniform or sparse) can provide better resolution and robustness, particularly for closely spaced angles. For example, linear sparse arrays can offer larger effective apertures with fewer sensors, providing better resolution for the same computational cost. To the best of the authors' knowledge, the challenge of improving the resolution accuracy of Direction of Arrival (DOA) estimation by strategically rearranging the RIS elements for closely spaced angular targets has not been explored in the literature. In this paper, we focus on Minimum Redundancy Linear Arrays (MRLAs) configure (the class of linear sparse arrays) to enhance the direction finding results using Binary-Phase Reconfigurable Intelligent Surface (Binary-Phase RIS) for closely spaced angles. The proposed methodology presents a significant advancement in DOA estimation, particularly for closely spaced targets, without introducing additional hardware complexity. This improvement enhances target resolution in challenging operational environments, which is fundamental for applications in wireless communication, radar systems, and the Internet of Things (IoT). The approach's cost-efficiency and enhanced accuracy contribute to the development of more sophisticated signal processing techniques, with profound implications for domains requiring high-precision angular estimation.

In essence, as mentioned before, the proposed approach does not require additional hardware compared to previous algorithms. Instead, it relies solely on altering the geometry of the RIS elements arrangement to enhance the resolution accuracy for closely spaced angular targets using MRLA concept. The seminal paper [11] introduced the concept of MRLAs, which achieve maximum unique spatial lags with the fewest possible elements. It laid the theoretical foundation for efficient array geometries that enhance angular resolution and reduce hardware complexity—principles directly utilized in our proposed RIS configuration.

In our solution, owing to Binary-Phase RIS, the atoms exhibit correlation. So, we also utilized the atomic norm for angle recovery as it does not require the atoms to be uncorrelated.

Notations: Boldface italic upper-case and lower-case letters represent matrices and column vectors, respectively. The symbols $(\cdot)^{T}$ and $(\cdot)^{H}$ denote the transpose and Hermitian transpose of a matrix, respectively.

2- MRLA Binary-Phased RIS-aided model for DOA estimation

Recently, there are some papers on RIS with sparse arrays or RIS with coprime arrays. In [12], a hybrid sparse-active RIS architecture (L-shaped sparse subarrays) is used for joint sensing and communication (ISAC), and they apply nuclear-norm based interpolation to fill in missing covariance entries for DOA estimation over the sparse RIS. A sparse Bayesian learning approach is developed in [13], with a neural unrolling architecture, for off-grid DOA estimation with one-bit quantization in non-uniform sparse arrays—demonstrating robustness in realistic quantized array contexts.

In the context of the MRLA binary-phased RIS-aided direction finding system, we employ NN RIS elements to construct a Sparse Linear Array (SLA), as illustrated in Fig.1.

There is an obstacle between both transmitters (target 1 and target 2) and a single antenna receiver.

However, the RIS, configured as an MRLA, maintains line-of-sight (LOS) with both transmitters and the receiver. As a result, it can receive the signals emitted by the transmitters and reflect them to the receiver. All the reflected signals from the RIS are received by a single antenna system at a fixed and known direction, denoted as ψ .

We assume the minimum distance between two adjacent MRLA binary-phased (MRLA-BP) RIS elements is half a wavelength, referred to as grid spacing *d*. Let *K* denote the number of targets, θ_k the direction of the *k*-th target towards the MRLA-BP RIS, and s_k the signal from the *k*-th target. It is noteworthy that MRLA belongs to a class of non-uniform linear arrays.

The MRLA employs a minimal number of elements within the array structure to generate all gaps between zero and a predefined maximum number (in this case, six, as shown in Fig. 1). The primary advantage of MRLA is its ability to construct the longest aperture in co-prime arrays while utilizing the least number of array elements. Consequently, it offers the highest resolution for separating closely spaced angular targets.

Fig. 2 illustrates the spatial spectrum for DOA estimation of two linear arrays: the uniform linear array (ULA) and the MRLA, for three targets with emission angles of -20°, 30.56°, and 32.24°. As depicted in Fig.2, only the MRLA is capable of distinguishing between the two nearly angularly close targets, whereas the ULA fails to do so, despite both arrays employing the same number of elements.

The 4-element MRLA depicted in Fig. 1 performs comparably to a standard ULA with a 7-element aperture. Specifically, a spatial delay of 1 is achieved by the element pair $\{P_0 = 0, P_1 = d\}$, a spatial delay of 2 by $\{P_2 = 4d, P_3 = 6d\}$,

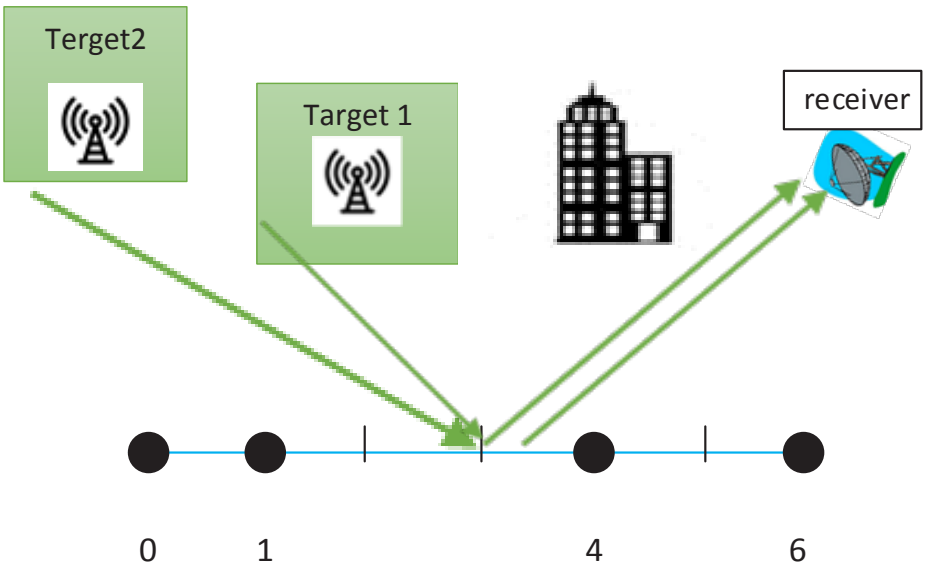

Fig. 1. The schematic model for Direction of Arrival (DOA) estimation using a one-dimensional MRLA RIS.

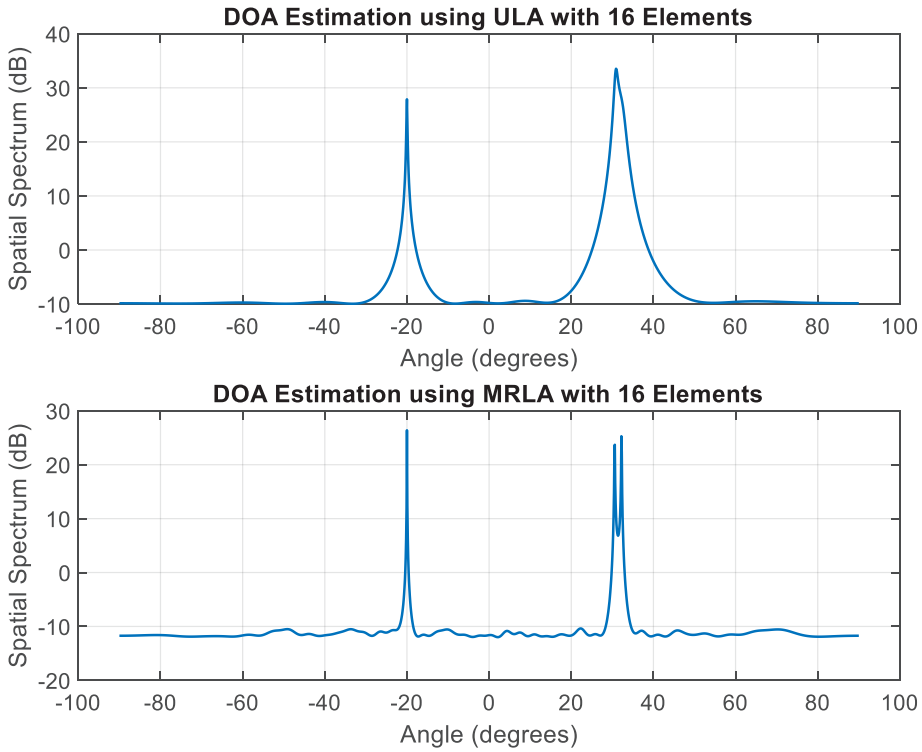

Fig. 2. The spatial spectrum for DOA estimation with ULA and MRLA for three targets at angles of -20°, 30.56°, and 32.24°. The detailed structure of the MRLA is discussed in the simulation section.

a spatial delay of 3 by $\{P_1 = d, P_2 = 4d\}$, a spatial delay of 4 by $\{P_0 = 0, P_2 = 4d\}$, a spatial delay of 5 by $\{P_1 = d, P_3 = 6d\}$, and finally, a spatial delay of 6 by $\{P_0 = 0, P_3 = 6d\}$.

Assume that the position of the n-th element of the MRLA-BP RIS is denoted as P_n. The emitted signals towards the MRLA-BP RIS during the m-th $(m = 0,1,\ldots,M-1)$ measurement snapshot are given by:

$$[e^{j\phi_{m,0}}\sum_{k=0}^{K-1}s_k e^{j2\pi\frac{P_0}{\lambda}\sin\theta_k}, e^{j\phi_{m,1}}\sum_{k=0}^{K-1}s_k e^{j2\pi\frac{P_1}{\lambda}\sin\theta_k}, \ldots \\ \ldots, e^{j\phi_{m,N-1}}\sum_{k=0}^{K-1}s_k e^{j2\pi\frac{P_{N-1}}{\lambda}\sin\theta_k}] \quad (1)$$

where $\phi_{m,n} \in \{0,\pi\}$ is a phase of the n-th MRLA binary-phased RIS element at m-th measurement. Restricting the phase quantization to only two levels significantly reduces implementation complexity; however, it inevitably imposes limitations on the achievable estimation accuracy [14]. s_k is the k-th target signal value during the m-th measurement. We assume that the values $\{s_k\}_{k=0}^{k-1}$ remain constant during the M snapshots. Therefore, the scalar m-th measurement received by the receiver can be written as:

$$r_m = \sum_{n=0}^{N-1}\left[e^{j\phi_{m,n}}\sum_{k=0}^{K-1}s_k e^{j2\pi\frac{P_n}{\lambda}\sin\theta_k}\right]e^{j2\pi\frac{P_n}{\lambda}\sin\psi} + w_m \quad (2)$$

Let w_m represent the AWG noise at the receiver. Suppose the positions of the MRLA-BP RIS elements are collected in the position vector $\mathbf{p} = [P_0, P_1, \ldots, P_{N-1}]^T$, the target's DOA in $\theta = [\theta_0, \theta_1, \ldots, \theta_{K-1}]^T$, $\mathbf{s}$ as $[s_0, s_1, \ldots, s_{K-1}]^T$, and the noise vector $\mathbf{w} = [w_0, w_1, \ldots, w_{M-1}]^T$. Then the M measurements at the receiver can be represented in matrix form as:

$$\mathbf{r} \triangleq \begin{bmatrix} r_0 \\ r_1 \\ \cdot \\ \cdot \\ \cdot \\ r_{M-1} \end{bmatrix} = \underbrace{\begin{bmatrix} e^{j\phi_{0,0}} & \cdots & e^{j\phi_{0,N-1}} \\ \vdots & \ddots & \vdots \\ e^{j\phi_{M-1,0}} & \cdots & e^{j\phi_{M-1,N-1}} \end{bmatrix}}_{\mathbf{U}} \quad (3)$$

$$\times \underbrace{\mathrm{diag}\left\{\begin{bmatrix} e^{j2\pi\frac{P_0}{\lambda}\sin\psi} & \cdots & e^{j2\pi\frac{P_{N-1}}{\lambda}\sin\psi} \end{bmatrix}^T\right\}}_{\mathbf{A}_2(\psi,\mathbf{p})}$$

$$\times \underbrace{\begin{bmatrix} e^{j2\pi\frac{P_0}{\lambda}\sin\theta_0} & \cdots & e^{j2\pi\frac{P_0}{\lambda}\sin\theta_{K-1}} \\ \vdots & \ddots & \vdots \\ e^{j2\pi\frac{P_{N-1}}{\lambda}\sin\theta_0} & \cdots & e^{j2\pi\frac{P_{N-1}}{\lambda}\sin\theta_{K-1}} \end{bmatrix}}_{\mathbf{A}_1(\boldsymbol{\theta},\mathbf{p})} \mathbf{s} + \mathbf{w}$$

Finally, we have:

$$\mathbf{r} \triangleq \mathbf{U}\mathbf{A}_2(\psi,\mathbf{p}).\mathbf{A}_1(\boldsymbol{\theta},\mathbf{p})\mathbf{s} + \mathbf{w} \quad (4)$$

where $\mathbf{U}$ is referred to as the MRLA-BP RIS measurement matrix.

It is important to note that the elements of the measurement matrix $\mathbf{U}$ are either -1 or +1. As $\mathbf{U}$ is a rectangular matrix rather than a square one, it is challenging to satisfy the Restricted Isometry Property (RIP) condition. This difficulty is particularly pronounced when the element values are chosen randomly, with no intention of adhering to the RIP in their design. In this study, the element values were also selected randomly.

3- Design and Optimization of an MRLA for Enhanced Precision

The principle behind employing MRLA for BP-RIS instead of the conventional uniform linear arrays (ULAs)—as commonly adopted in the literature—is to improve DOA estimation accuracy for closely spaced targets, while maintaining the existing hardware complexity.

The aim of this section is to systematically choose an MRLA configuration by proposing an optimization criterion that captures key objectives, such as maximizing the number of unique inter-element spacings, minimizing redundancy, and adhering to physical constraints—specifically, maintaining a minimum spacing of at least half a wavelength to ensure signal integrity and array performance.

The MRLA consists of N elements at positions $\mathbf{p} = [P_0, P_1, \ldots, P_{N-1}]^T$. We must first define a metric that counts the number of unique spacings for the given configuration $\mathbf{p}$. For every pair of elements (P_i, P_j) with $i < j$, we define the spacing (lag):

$$d_{ij} = |P_i - P_j| \quad (5)$$

To use a metric defining the set of unique lags, let $\mathfrak{D}$ be the set of all such pairwise spacings:

$$\mathfrak{D}(\mathbf{p})=\left\{\left|P_i-P_j\right|:0\le i<j\le N-1\right\} \tag{6}$$

As the cardinality of a set refers to the size of the set, or the number of distinct elements it contains, the cardinality of this set, $\left|\mathfrak{D}(\mathbf{p})\right|$, is the number of unique lags. Finally, the optimization problem of finding the best MRLA configuration, $\mathbf{p}^*$, is formulated as follows subject to spacing and physical constraints:

$$\begin{aligned}&\mathbf{p}^*=\arg\max_{\mathbf{p}\in\mathfrak{P}}\left|\mathfrak{D}(\mathbf{p})\right|,\\&\text{subject to}\left|P_i-P_{i+1}\right|\ge\frac{\lambda}{2},0\le i\le N-2,\end{aligned} \tag{7}$$

Here, $\mathfrak{P}$ represents the set of all feasible configurations and λ is the wavelength.

To ensure the solvability of the problem (7), the minimum spacing between adjacent array elements is set to half a wavelength. Additionally, it is assumed that the candidate positions for placing the array elements are integer multiples of half a wavelength:

$$P_i=\kappa_i\frac{\lambda}{2} \tag{8}$$

where each $\kappa_i\in\mathbb{Z}^+$ denotes the slot index, where $\mathbb{Z}^+$ is the set of positive integers.

Moreover, the maximum length of the MRLA is constrained within a specified limit, such as $L_{\max}$, to account for practical considerations and implementation feasibility.

So, the optimization problem in (7) changes to:

$$\begin{aligned}&\boldsymbol{\kappa}^*=\arg\max_{\boldsymbol{\kappa}\in\mathbb{Z}^{+N}}\left|\mathfrak{D}\left(\frac{\lambda}{2}\boldsymbol{\kappa}\right)\right|,\\&\text{subject to:}\\&\left|\kappa_i-\kappa_{i+1}\right|\ge1,0\le i\le N-2,\\&\max(\boldsymbol{\kappa})-\min(\boldsymbol{\kappa})\le L_{\max}.\end{aligned} \tag{9}$$

Here, $\mathbb{Z}^{+N}$ represents the vector of N elements each belong to the set of positive integers.

Since the $\left|\mathfrak{D}\left(\frac{\lambda}{2}\kappa\right)\right|$ operator is both non-convex and non-differentiable, the problem (9) falls into the category of combinatorial optimization. To solve it, several approaches can be employed, including: 1) Integer programming, which is suitable for small grid sizes where exhaustive computation is feasible [15] , [16]. 2) Greedy search or heuristic methods, which provide approximate solutions efficiently by leveraging problem-specific strategies [17],[18]. 3) Genetic algorithms, which utilize evolutionary principles to explore the solution space and converge toward optimal configurations[19].

For the sake of simplicity and ease of implementation in software coding, the greedy search method is employed to determine the optimal MRLA configuration, as outlined in Section 4.

4- Analytical Justification of the Greedy Algorithm to Determine the Optimal MRLA Configuration

This section provides a precise mathematical justification for employing a greedy search algorithm to maximize the number of unique inter-element spacings, ensuring an optimal array configuration.

Suppose $\min(\kappa)=0$ and let $\mathfrak{G}=\{0,1,\cdots,L_{\max}\}$ be the allowable element-slot indices (in units of $\lambda/2$). For any N-element subset $\kappa\subset\mathfrak{G}$, define $f(\kappa)=\left|\mathfrak{D}\left(\frac{\lambda}{2}\kappa\right)\right|$, as the total number of unique inter-element spacings, where $\mathfrak{D}$ is defined in (6) with consideration of (8). We wish to select an N-element subset

$$\boldsymbol{\kappa}=\left\{\kappa_0,\cdots,\kappa_{N-1}\right\}\subset\mathfrak{G}, \tag{10}$$

so as to maximize the number of unique inter-element spacings. Define the set of all pairwise lags of κ as $\mathfrak{D}\left(\frac{\lambda}{2}\kappa\right)$. The objective is $f(\kappa)=\left|\mathfrak{D}\left(\frac{\lambda}{2}\kappa\right)\right|$.

By construction, $f(\phi)=0$ and f is integer-valued and nondecreasing: if $\kappa\subset Q\subset\mathfrak{G}$, then $\mathfrak{D}\left(\frac{\lambda}{2}\kappa\right)\subset\mathfrak{D}\left(\frac{\lambda}{2}Q\right)$, so $f(\kappa)\le f(Q)$.

For any current partial selection $S\subset\mathfrak{G}$ and any candidate $x\in\mathfrak{G}\setminus S$, define the marginal gain:

$$\Delta(x\mid S)=f\left(S\cup\{x\}\right)-f(S), \tag{11}$$

Concretely, if $S=\{\kappa_0,\cdots,\kappa_{k-1}\}$, then

$$\begin{aligned}&\Delta(x\mid S)=\\&\left|\left\{\left|\kappa_i-\kappa_j\right|;\ 0\le i<j\le k-1\right\}\cup\left\{\left|x-\kappa_i\right|:\ i=0,\cdots,k-1\right\}\right|\\&-\left|\left\{\left|\kappa_i-\kappa_j\right|;0\le i<j\le k-1\right\}\right|\end{aligned} \tag{12}$$

Intuitively, $\Delta(x\mid S)$ counts how many new lags $|x-\kappa_i|$ (for $i=0,\cdots,k-1$) are not already present among the $f(S)$ distinct lags.

We can show that f satisfies a diminishing-returns (submodularity) property:

$$\triangle(x \mid A) \geq \triangle(x \mid B) \text{ whenever } A \subseteq B \subset \mathfrak{G}, x \notin B. \quad (13)$$

In other words, adding a new element x to a smaller set A can only produce as many or more "new spacings" than adding it to a larger set B. Because if B already contains more elements, many of the potential lags $|x-b|$ may already be "covered" in $\mathfrak{D}\left(\frac{\lambda}{2}B\right)$.

A standard greedy algorithm builds κ one element at a time. At step k, suppose we have already chosen

$$S_{k-1} = \{\kappa_0, \cdots, \kappa_{k-1}\}. \quad (14)$$

We pick the next element κ_k to maximize the marginal gain:

$$\kappa_k = \arg \max_{x \in \mathfrak{G} \setminus S_{k-1}} \triangle(x \mid S_{k-1}). \quad (15)$$

Thus each iteration greedily chooses the slot x whose addition yields the largest increase in the count of unique spacings. Denote the resulting set of size N by

$$\boldsymbol{\kappa}_{\text{greedy}} = \{\kappa_0, \cdots, \kappa_{N-1}\}. \quad (16)$$

Since f *is* nondecreasing and exhibits the diminishing-returns property, it is a submodular set function. A well-known result from submodular optimization (Nemhauser–Wolsey theorem [20]) says that, under a cardinality constraint $|\kappa| < N$, the greedy solution κ_{greedy} satisfies

$$f(\boldsymbol{\kappa}_{\text{greedy}}) \geq \left(1 - \frac{1}{e}\right) f(\boldsymbol{\kappa}^*). \quad (17)$$

where κ^* is the (NP-hard) exact maximizer of $f(\kappa)$ over all $\binom{|\mathfrak{G}|}{N}$ choices. In other words, the greedy algorithm is guaranteed to achieve at least $0.632 f(\kappa^*)$.

5- Grid-free DOA Estimation Using Atomic Norm Optimization

Traditional high-resolution DOA estimation methods such as MUSIC [21] and ESPRIT [22] have long served as foundational techniques in array signal processing. These subspace-based estimators exploit the orthogonality between the signal and noise subspaces to achieve angular super resolution, yet their performance strongly depends on accurate model order selection, sufficient snapshots, and high SNR conditions. [23] Provides a theoretical analysis of spatial smoothing techniques, which are fundamental in handling correlated sources and sparse array geometries.

In contrast, the atomic-norm-based framework introduces a gridless and convex formulation for DOA estimation, effectively overcoming the basis mismatch and discretization errors inherent to grid-based or subspace methods.

The atomic norm is a convex measure that represents the smallest weighted combination of basic building blocks—called atoms—needed to express a signal. It promotes sparsity by encouraging representations using as few atoms as possible from a predefined atomic set.

By directly promoting spectral sparsity in the continuous domain, atomic norm minimization enables super-resolution recovery of closely spaced sources even under low-SNR or hardware-constrained scenarios, thereby offering a significant advantage—especially within our proposed MRLA-RIS architecture, where binary-phase limitations and limited measurements make conventional subspace methods less effective.

Given that dictionary learning is less critical when using the atomic norm, the atomic norm can be incorporated as a regularization component within the cost function of the optimization problem to determine DOAs as follows:

$$\min_{\gamma} \frac{1}{2} \left\| \mathbf{U}\mathbf{A}_2(\psi, \mathbf{p}).\boldsymbol{\gamma} - \mathbf{r} \right\|_2^2 + \varepsilon \|\boldsymbol{\gamma}\|_{\mathcal{A}} \quad (18)$$

where ε is the regularization parameter controlling the sparsity level as well as recovering accuracy and the atomic norm $\|\gamma\|_{\mathcal{A}}$ is defined as:

$$\|\boldsymbol{\gamma}\|_{\mathcal{A}} = \inf \left\{ \begin{array}{l} \sum_{n=0}^{N-1} |c_n| : \\ \boldsymbol{\gamma} = \sum_{n=0}^{N-1} c_n \mathbf{A}_1(\theta_n, \mathbf{p}), \\ \theta_n \in \left(-\frac{\pi}{2}, \frac{\pi}{2}\right] \end{array} \right\} \quad (19)$$

As can be seen from the definition of $\|\gamma\|_{\mathcal{A}}$, the unknown θ_n could be any angle in $\left(-\frac{\pi}{2}, \frac{\pi}{2}\right]$, where $\mathbf{A}_1(\theta_n, \mathbf{p})$ denotes the n-th column of $A_1(\theta, p)$, and θ is replaced with the unknown θ_n (It is assumed that $\mathbf{p}$ is precisely known upon solving the optimization problem (18).)

If we position the receiver such that $\psi = 0$, then $\mathbf{A}_2(\psi, \mathbf{p}) = \mathbf{I}_N$ where $\mathbf{I}_N$ is the identity matrix of size N, and the notations are simplified. Additionally, N represents the virtual aperture size of the MRLA-binary-phased RIS (which is 6 in Fig. 1).

The problem (18) can be rewritten as

$$\min_{\boldsymbol{\gamma},\boldsymbol{\alpha}} \frac{1}{2}\left\|\boldsymbol{\alpha}-\mathbf{r}\right\|_2^2+\varepsilon\left\|\boldsymbol{\gamma}\right\|_{\mathcal{A}} \;\; s.t\, \boldsymbol{\alpha}=\mathbf{U}\mathbf{A}_2\left(\psi,\mathbf{p}\right).\boldsymbol{\gamma} \quad (20)$$

where its Lagrangian function is obtained as:

$$\begin{aligned}\mathcal{L}\left(\boldsymbol{\alpha},\boldsymbol{\gamma},\boldsymbol{\beta}\right)=&\frac{1}{2}\left\|\boldsymbol{\alpha}-\mathbf{r}\right\|_2^2+\varepsilon\left\|\boldsymbol{\gamma}\right\|_{\mathcal{A}}\\&+\boldsymbol{\beta}^{\boldsymbol{T}}\;\boldsymbol{\alpha}\left(-\mathbf{U}\mathbf{A}_2\left(\psi,\mathbf{p}\right).\boldsymbol{\gamma}\right)\end{aligned} \quad (21)$$

where β represents the Lagrange multipliers vector corresponding to the equality constraint $\alpha=\mathbf{U}\mathbf{A}_2\left(\psi,\mathbf{p}\right).\gamma$.

The dual function $g(\beta)$ is defined as the infimum of the Lagrangian with respect to the primal variables γ and α.

$$\begin{aligned}&g\left(\boldsymbol{\beta}\right)=\inf_{\boldsymbol{\alpha},\boldsymbol{\gamma}}\mathcal{L}\left(\boldsymbol{\alpha},\boldsymbol{\gamma},\boldsymbol{\beta}\right)=\\&\inf_{\boldsymbol{\alpha}}\left(\frac{1}{2}\left\|\boldsymbol{\alpha}-\mathbf{r}\right\|_2^2+\boldsymbol{\beta}^{\boldsymbol{T}}\;\boldsymbol{\alpha}\right)\\&+\inf_{\boldsymbol{\gamma}}(\varepsilon\left\|\boldsymbol{\gamma}\right\|_{\mathcal{A}}-\boldsymbol{\beta}^{\boldsymbol{T}}\mathbf{U}\mathbf{A}_2\left(\psi,\mathbf{p}\right).\boldsymbol{\gamma})=\\&\frac{1}{2}\left(\left\|\mathbf{r}\right\|_2^2-\left\|\mathbf{r}-\boldsymbol{\beta}\right\|_2^2\right)\\&+\sup_{\boldsymbol{\gamma}}(\boldsymbol{\beta}^{\boldsymbol{T}}\mathbf{U}\mathbf{A}_2\left(\psi,\mathbf{p}\right).\boldsymbol{\gamma}-\varepsilon\left\|\boldsymbol{\gamma}\right\|_{\mathcal{A}})\end{aligned} \quad (22)$$

The Lagrangian is always concave because it is the pointwise infimum of a family of affine functions. Therefore, the dual problem is formulated as follows:

$$\max_{\boldsymbol{\beta}} g\left(\boldsymbol{\beta}\right)=\max_{\boldsymbol{\beta}}\min_{\boldsymbol{\alpha},\boldsymbol{\gamma}}\mathcal{L}\left(\boldsymbol{\alpha},\boldsymbol{\gamma},\boldsymbol{\beta}\right) \quad (23)$$

So the dual problem becomes

$$\begin{aligned}&\max_{\boldsymbol{\beta}}\left[\begin{array}{l}\frac{1}{2}\left(\left\|\mathbf{r}\right\|_2^2-\left\|\mathbf{r}-\boldsymbol{\beta}\right\|_2^2\right)\\+\max_{\boldsymbol{\gamma}}(\boldsymbol{\beta}^{\boldsymbol{T}}\mathbf{U}\mathbf{A}_2\left(\psi,\mathbf{p}\right).\boldsymbol{\gamma}-\varepsilon\left\|\boldsymbol{\gamma}\right\|_{\mathcal{A}})\end{array}\right]=\\&\min_{\boldsymbol{\beta}}\frac{1}{2}\left(\left\|\mathbf{r}-\boldsymbol{\beta}\right\|_2^2\right)\\&+\max_{\boldsymbol{\beta},\boldsymbol{\gamma}}\left(\boldsymbol{\beta}^{\boldsymbol{T}}\mathbf{U}\mathbf{A}_2\left(\psi,\mathbf{p}\right).\boldsymbol{\gamma}-\varepsilon\left\|\boldsymbol{\gamma}\right\|_{\mathcal{A}}\right)\end{aligned} \quad (24)$$

Suppose that $\mathbf{C}\triangleq\mathbf{U}\mathbf{A}_2\left(\psi,\mathbf{p}\right)$. Utilizing a Lagrange duality technique and converting the soft constraint into a hard constraint, the second term on the right-hand side of (24) is equivalent to:

$$\begin{aligned}&\min_{\boldsymbol{\beta},\boldsymbol{\gamma}}\left(-\boldsymbol{\gamma}^{\boldsymbol{H}}\mathbf{C}^{\boldsymbol{H}}\boldsymbol{\beta}+\varepsilon\left\|\boldsymbol{\gamma}\right\|_{\mathcal{A}}\right)=\\&\min_{\boldsymbol{\beta},\boldsymbol{\gamma},\left\|\boldsymbol{\gamma}\right\|_{\mathcal{A}}\le\tau}\left(-\boldsymbol{\gamma}^{\boldsymbol{H}}\mathbf{C}^{\boldsymbol{H}}\boldsymbol{\beta}\right),\end{aligned} \quad (25)$$

where τ is unique such that there exists an equivalent τ that ensures both the right-hand side and the left-hand side of (25) yield the same solution. The optimization problem (25) with a hard constraint can be transformed into:

$$\min_{\boldsymbol{\beta},\boldsymbol{\gamma},\left\|\boldsymbol{\gamma}\right\|_{\mathcal{A}}\le\tau}-\left\langle\boldsymbol{\gamma},\mathbf{C}^{\boldsymbol{H}}\boldsymbol{\beta}\right\rangle=\max_{\boldsymbol{\beta},\boldsymbol{\gamma},\left\|\boldsymbol{\gamma}\right\|_{\mathcal{A}}\le\tau}\left\langle\boldsymbol{\gamma},\mathbf{C}^{\boldsymbol{H}}\boldsymbol{\beta}\right\rangle \quad (26)$$

By expanding (26) based on the definition of the atomic norm, it can be written as:

$$\begin{aligned}&\max_{\boldsymbol{\beta}}\left(\sum_n Re\left\{c_n^{*}\mathbf{A}_1^{H}\left(\theta_n,\mathbf{p}\right)\mathbf{C}^{\boldsymbol{H}}\boldsymbol{\beta}\right\}\right)\\&\quad s.t\;\theta_n\in\left(-\frac{\pi}{2},\frac{\pi}{2}\right],\sum_{n=0}^{N-1}\left|c_n\right|\le\tau\\\le&\max_{\boldsymbol{\beta}}\left(\sum_n\left|c_n\right|\left|\mathbf{A}_1^{H}\left(\theta_n,\mathbf{p}\right)\mathbf{C}^{\boldsymbol{H}}\boldsymbol{\beta}\right|\right)\\&\quad s.t\;\theta_n\in\left(-\frac{\pi}{2},\frac{\pi}{2}\right],\sum_{n=0}^{N-1}\left|c_n\right|\le\tau\\\le&\tau\max_{\boldsymbol{\beta}}\left|\mathbf{A}_1^{H}\left(\theta_n,\mathbf{p}\right)\mathbf{C}^{\boldsymbol{H}}\boldsymbol{\beta}\right|\\&\quad s.t\;\;\theta_n\in\left(-\frac{\pi}{2},\frac{\pi}{2}\right]\\&\max_{\boldsymbol{\beta},\left\|\boldsymbol{\gamma}\right\|_{\mathcal{A}}\le1}sup\left\langle\tau\mathbf{A}_1\left(\theta,\mathbf{p}\right),\mathbf{C}^{\boldsymbol{H}}\boldsymbol{\beta}\right\rangle\\=&\tau\max_{\boldsymbol{\beta}}\left\|\mathbf{C}^{\boldsymbol{H}}\boldsymbol{\beta}\right\|_{\tilde{\mathcal{A}}}\end{aligned} \quad (27)$$

where $\left\|\beta\right\|_{\tilde{\mathcal{A}}}\triangleq\sup_{\left\|\gamma\right\|_{\mathcal{A}}\le1}\left\langle\beta,\gamma\right\rangle$ represents the dual norm of the atomic norm. Thus, the optimization problem (24) becomes:

$$\min_{\boldsymbol{\beta}} \frac{1}{2}\left(\left\|\mathbf{r}-\boldsymbol{\beta}\right\|_2^2\right)+\tau \max_{\boldsymbol{\beta}} \left\|\mathbf{C}^{H}\boldsymbol{\beta}\right\|_{\tilde{\mathcal{A}}} \tag{28}$$

By again employing the dual Lagrangian and transforming the soft constraint into a hard constraint, (28) can be converted into:

$$\min_{\boldsymbol{\beta}} \frac{1}{2}\left(\left\|\mathbf{r}-\boldsymbol{\beta}\right\|_2^2\right) \;\; s.t \;\; \left\|\mathbf{C}^{H}\boldsymbol{\beta}\right\|_{\tilde{\mathcal{A}}} \le \varepsilon, \tag{29}$$

where the hard constraint on the dual atomic norm is applied to ε .The value of the hyper parameter ε can be set as $\sqrt{10^{0.1SNR}}.MK.\log MK$ [6]. The optimization problem (29) can be readily solved by CVX package in MATLAB, with a computational complexity of $\mathcal{O}\left(N^{3.5}\right)$. The final solution can be obtained by peak picking in $f\left(\theta\right)=\left\langle C^{H}\beta, A_1\left(\theta,p\right)\right\rangle$ in terms of θ.

6- Simulation Results

In this section, the performance of signal direction of arrival (DOA) estimation using the MRLA-BP RIS is evaluated by comparing it with the results of three algorithms presented in [4], [6] and [24]. In [4], after optimization using the genetic algorithm, a matrix **U** with 16 columns and 20 rows was employed. Similarly, in our proposed MRLA method, the number of physical elements is set to 16 for a fair comparison. The inter-element spacing *d* is set to half the wavelength, and simulations are conducted for two different scenarios. In the first scenario, three targets are considered, with two positioned at closely spaced angles, specifically at $-20^{\circ}, 30.56^{\circ}$, and 32.24°. In the second scenario, three clearly distinct targets are located at angles $-20^{\circ}, 0^{\circ}$, and 32.24° .The number of measurement snapshots is set to 20 for both scenarios. The method used in [24] is called l1 singular value decomposition (l1-SVD) where the received signals are modeled as a linear combination of steering vectors from a dense grid of possible source directions and to handle multiple snapshots (i.e., time samples), the method applies Singular Value Decomposition (SVD) to the data matrix and then the sparse recovery problem is formulated as a second-order cone programming (SOCP) problem.

For an MRLA configuration with an aperture consisting of 16 real elements, multiple possible combinations of physical elements exist. To determine an optimal configuration of $\mathbf{p}$, we employ the greedy search method outlined in Section 3. Specifically, we set $\min\left(\kappa\right)=0$ and compute $\mathbf{p}^{*}$ for $\max\left(\kappa\right)=L_{\max}=40$.

Applying the greedy algorithm, for example, results in the following possible configuration of physical element positions for $L_{\max}=40$: ([0*d*, 4*d*, 6*d*, 10*d*, 12*d*, 15*d*, 18*d*, 20*d*, 23*d*, 25*d*, 29*d*, 31*d*, 34*d*, 38*d*, 40*d*]), focusing on a configuration that uses 16 physical elements within the 40 slots to maximize unique inter-element spacings. The corresponding pairs of positions and delays for the given MRLA array are shown in Table 1. There are a total of 120 unique delay values.

Figs. 3 and 4 present the performance of the algorithms under two distinct scenarios: (1) when two out of three targets are closely spaced in the angular domain, and (2) when all three targets are well-separated. The results in these figures represent the average over 1000 independent trials for each setup.

In general, as the SNR increases, the performance of all algorithms improves in both scenarios, with sharper RMSE reductions for the proposed method and Ref. [4]. However, the angular estimation accuracy is notably lower for all algorithms in the first scenario (closely spaced targets) compared to the second scenario (well-separated targets). This behavior aligns with expectations, as resolving closely spaced targets is inherently more challenging.

Notably, in both scenarios, the proposed algorithm outperforms all other algorithms. In closely spaced scenario, the RMSE significantly decreases as the SNR increases, reaching a very low value (0.3351degrees) at $30\,\mathrm{dB}$. This indicates that the proposed method demonstrates strong robustness against noise and achieves high accuracy at high SNR levels. For well-separated target scenarios, the RMSE decreases rapidly with increasing SNR, achieving an extremely low value of 0.0359 degrees at $30\,\mathrm{dB}$.

The superior performance of Ref. [4] compared to Ref. [6] and l1-SVD in both Figures 3 and 4 is due to the use of a genetic algorithm to optimize the RIS observation matrix **U**. However, as evident from the Figs. 3 and 4, the improvement achieved by Ref. [4] is less significant than that obtained through the proper arrangement of RIS elements in our proposed algorithm. It is worth mentioning that in our proposed algorithm, the RIS elements are randomly selected from $\{\pm 1\}$, and no optimization efforts were made regarding the selection of the **U** matrix.

As illustrated in both Fig. 3 and Fig. 4, the performance of the l1-SVD method falls short of that achieved by the approach in Ref. [4], and even more so when compared to our proposed method. This discrepancy arises from the inherent limitations of grid-based techniques such as l1-SVD, where the angular domain is discretized into dense grids. Such discretization increases the coherence of the measurement matrix, thereby degrading the recovery performance. In contrast, gridless approaches—such as the atomic norm minimization employed in Ref. [4]—demonstrate superior performance under these conditions. It is also noteworthy that the l1-SVD method consistently outperforms the technique presented in Ref. [6] across both scenarios, including cases with $\sigma=0.02$ and $\sigma=0.2$. This observation suggests that even gridless methods, as in Ref. [6], may struggle to maintain robustness when the RIS element locations are subject to uncertainty, whereas dense grid-based methods like l1-SVD can still offer competitive performance.

Additionally, the angular estimation performance of Ref. [6] with a standard deviation (STD) of positional uncertainty of 0.02 outperforms Ref. [6] with $\sigma=0.2$, as the STD is ten times higher. Ref. [6] shows poorer performance in the closely spaced target scenario, but performs relatively better in the well-separated target scenario.

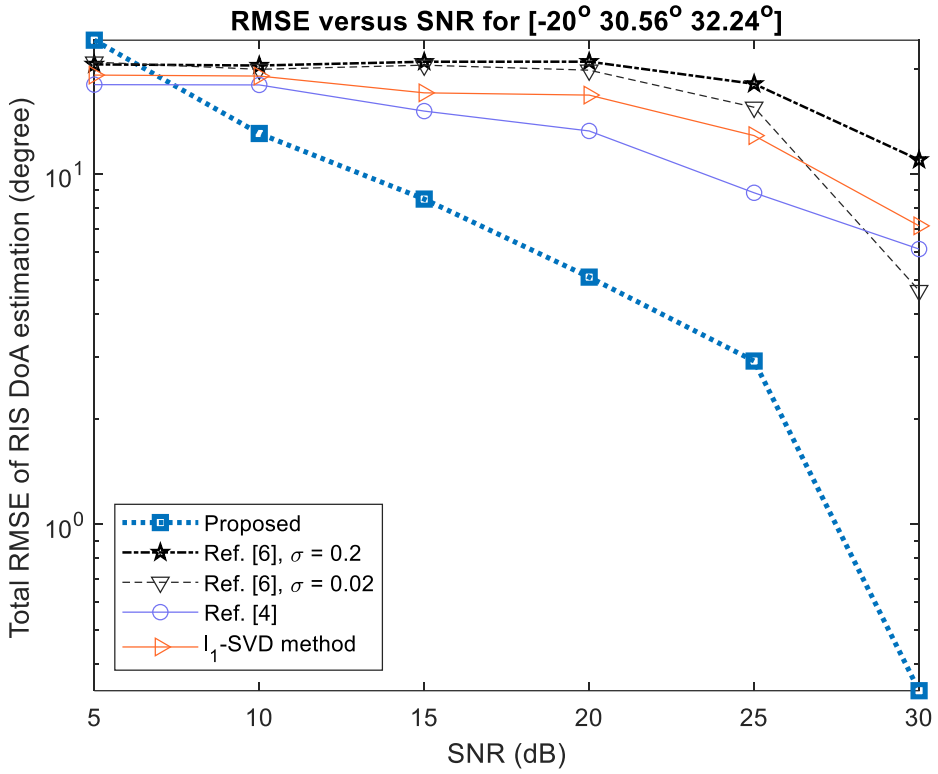

Fig. 3. The RMSE of the DOA estimation across various SNR levels, considering scenarios where two of the three targets have closely spaced angles.

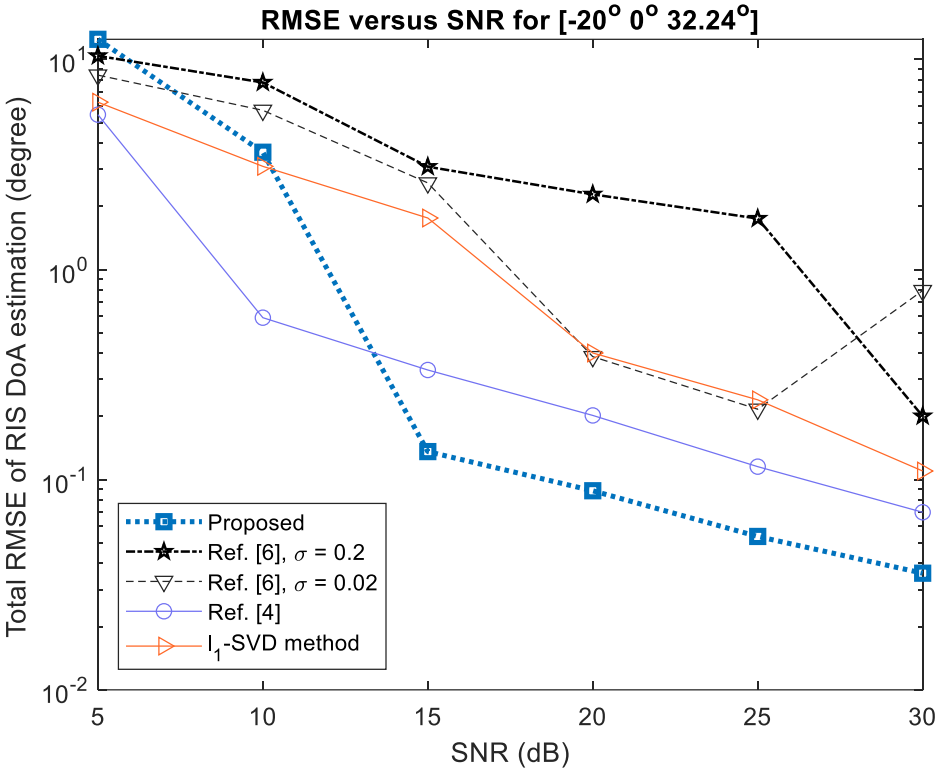

Fig. 4. The RMSE of the DOA estimation across various SNR levels, considering scenarios where all three targets are widely separated in the angular domain.

Table 1. MRLA Elements' position and their corresponding lags.

Position of the MRLA elements	Delays in terms of d
0-1	1d
0-4	$4d$
0-6	$6d$
0-10	$10d$
0-12	$12d$
…	…
34-38	$4d$
34-40	$6d$
38-40	$2d$

7- Conclusion

This study introduced a novel method for enhancing DOA estimation accuracy using a Binary-Phase Reconfigurable Intelligent Surface (Binary-Phase RIS) configured as a Minimum Redundancy Linear Array (MRLA). The proposed algorithm outperformed existing methods, achieving almost the lowest RMSE across various SNR levels in both closely spaced and well-separated target scenarios, particularly excelling in resolving closely spaced angular targets where other algorithms faced significant challenges. Unlike some existing methods that rely on complex optimization of the RIS measurement matrix, the proposed approach leverages a simple and efficient configuration of RIS elements, randomly selected from $\{\pm 1\}$, to achieve superior accuracy without additional hardware complexity. The results highlight the critical role of properly arranging RIS elements to maximize spatial resolution, particularly in challenging scenarios with closely spaced targets. This underscores the potential of MRLAs to achieve desirable performance by maximizing unique inter-element spacings.

References

[1] Y. Liu et al., "Reconfigurable intelligent surfaces: Principles and opportunities," IEEE communications surveys & tutorials, vol. 23, no. 3, pp. 1546–1577, 2021.

[2] T. Ma, Y. Xiao, X. Lei, L. Zhang, Y. Niu, and G. K. Karagiannidis, "Reconfigurable intelligent surface-assisted localization: Technologies, challenges, and the road ahead," IEEE Open Journal of the Communications Society, vol. 4, pp. 1430–1451, 2023.

[3] A. Albanese, F. Devoti, V. Sciancalepore, M. Di Renzo, and X. Costa-Pérez, "MARISA: A self-configuring metasurfaces absorption and reflection solution towards 6G," in IEEE INFOCOM 2022-IEEE Conference on Computer Communications, 2022: IEEE, pp. 250–259.

[4] Z. Yang, P. Chen, Z. Guo, and D. Ni, "Low-cost beamforming and DOA estimation based on one-bit reconfigurable intelligent surface," IEEE Signal Processing Letters, vol. 29, pp. 2397–2401, 2022.

[5] P. Chen, Z. Chen, Z. Cao, and X. Wang, "A new atomic norm for DOA estimation with gain-phase errors," IEEE Transactions on Signal Processing, vol. 68, pp. 4293–4306, 2020.

[6] P. Chen, Z. Yang, Z. Chen, and Z. Guo, "Reconfigurable intelligent surface aided sparse DOA estimation method with non-ULA," IEEE Signal Processing Letters, vol. 28, pp. 2023–2027, 2021.

[7] F. Wen, H. Wang, G. Gui, H. Sari, and F. Adachi, "Polarized intelligent reflecting surface aided 2D-DOA estimation for NLoS sources," IEEE Transactions on Wireless Communications, vol. 23, no. 7, pp. 8085–8098, 2024.

[8] Y. Tian, Y. Feng, W. Liu, H. Chen, and G. Wang, "Reconfigurable intelligent surface aided DOA estimation by a single receiving antenna," IEEE Transactions on Communications, 2024.

[9] Y. Zheng, Q. Wang, L. Ren, Z. Ma, and P. Fan, "RIS aided gridless 2D-DOA estimation via decoupled atomic norm minimization," IEEE Transactions on Vehicular Technology, vol. 73, no. 10, pp. 15733–15738, 2024.

[10] Y. Azhdari and M. Farhang, "Neural Network-Based RIS Assisted NLoS DoA Estimation," arXiv e-prints, p. arXiv: 2406.18306, 2024.

[11] A. Moffet, "Minimum-redundancy linear arrays," IEEE Transactions on antennas and propagation, vol. 16, no. 2, pp. 172–175, 1968.

[12] M. Asif Haider, Y. D. Zhang, and E. Aboutanios, "ISAC system assisted by RIS with sparse active elements," EURASIP Journal on Advances in Signal Processing, vol. 2023, no. 1, p. 20, 2023.

[13] Y. Hu, S. Sun, and Y. D. Zhang, "Enhancing Off-Grid One-Bit DOA Estimation with Learning-Based Sparse

Bayesian Approach for Non-Uniform Sparse Array," in 2024 58th Asilomar Conference on Signals, Systems, and Computers, 2024: IEEE, pp. 577–582.

[14] H. Chen and P. K. Varshney, "Performance limit for distributed estimation systems with identical one-bit quantizers," IEEE Transactions on Signal Processing, vol. 58, no. 1, pp. 466–471, 2009.

[15] B. FRIEDLANDER, "Direction Finding Using Spatial Smoothing with Interpolated arrays," IEEE Trans., vol. 42, no. 5, pp. 613–620, 1994.

[16] R. Rajamäki and V. Koivunen, "Sparse sensor arrays for active sensing: Models, configurations, and applications," Sparse Arrays for Radar, Sonar, and Communications, pp. 273–299, 2024.

[17] P. Pal and P. P. Vaidyanathan, "Nested arrays: A novel approach to array processing with enhanced degrees of freedom," IEEE Transactions on Signal Processing, vol. 58, no. 8, pp. 4167–4181, 2010.

[18] S. Wang, S. Li, A. Hoorfar, K. Miao, G. Zhao, and H. Sun, "Compressive sensing-based sparse MIMO array synthesis for wideband near-field millimeter-wave imaging," IEEE Transactions on Aerospace and Electronic Systems, vol. 59, no. 6, pp. 7681–7697, 2023.

[19] R. L. Haupt, "Thinned arrays using genetic algorithms," IEEE transactions on antennas and propagation, vol. 42, no. 7, pp. 993–999, 1994.

[20] R. Iyer, N. Khargonkar, J. Bilmes, and H. Asnani, "Generalized submodular information measures: Theoretical properties, examples, optimization algorithms, and applications," IEEE Transactions on Information Theory, vol. 68, no. 2, pp. 752–781, 2021.

[21] R. Schmidt, "Multiple emitter location and signal parameter estimation," IEEE transactions on antennas and propagation, vol. 34, no. 3, pp. 276–280, 1986.

[22] R. H. Roy III and T. Kailath, "ESPRIT--Estimation of signal parameters via rotational invariance techniques," Optical Engineering, vol. 29, no. 4, pp. 296–313, 1990.

[23] A. J. Weiss and B. Friedlander, "Performance analysis of spatial smoothing with interpolated arrays," in [Proceedings] ICASSP 91: 1991 International Conference on Acoustics, Speech, and Signal Processing, 1991: IEEE, pp. 1377–1380.

[24] D. Malioutov, M. Cetin, and A. S. Willsky, "A sparse signal reconstruction perspective for source localization with sensor arrays," IEEE transactions on signal processing, vol. 53, no. 8, pp. 3010–3022, 2005.

HOW TO CITE THIS ARTICLE

M. Raees Danaee, A. Ataei, High-Precision Direction of Arrival Estimation for Closely Spaced Targets Using Binary-Phase Reconfigurable Intelligent Surfaces and Minimum Redundancy Linear Arrays , AUT J. Elec. Eng., 58(Special Issue 1) (2026) 27-38.

DOI: 10.22060/eej.2025.24292.5674